European Polymer Journal 112 (2019) 433–441

Contents lists available at ScienceDirect

European Polymer Journal

journal homepage: www.elsevier.com/locate/europolj

Synthesis and characterization of different sodium hyaluronate nanoparticles to transport large neurotherapeutic molecules through blood brain barrier after stroke

Sebastián Peralta[a], Santos Blanco[b], Raquel Hernández[b], Herminia Castán[a], Eva Siles[b], Esther Martínez-Lara[b], María Encarnación Morales[a], María Ángeles Peinado[b,*], María Adolfina Ruiz[a]

[a] Pharmacy and Pharmaceutical Technology Department, School of Pharmacy, University of Granada, Campus de Cartuja s/n., 18071 Granada, Spain
[b] Department of Experimental Biology, University of Jaén, Building B3, Campus de Las Lagunillas, S/N-23071 Jaén, Spain

ARTICLE INFO

Keywords:
Sodium hyaluronate
Nanoparticles
Blood brain barrier
Drugs delivery system
Stroke

ABSTRACT

Some biological drugs with proven neuroprotective capacity are unable to cross the blood brain barrier (BBB), preventing its use in neuroregenerative diseases such as stroke. The use of nanoparticles as a delivery system to transport large therapeutic molecules to the cerebral parenchyma may be a good option to overcome this limitation.

To achieve this goal, we have designed some polymer nanoparticles (NPs) by two ionic gelation methods of synthesis: external (M1) and internal (M2), both using sodium hyaluronate (SH) as polymer but with differences in the elaboration of their core. Additionally, both SH-NPs were coated with chitosan and glycerol tripalmitin in order to improve their penetration capabilities into cells. The nanoparticles were characterized by size, shape and charge. Then, an experimental approach was carried out in animals submitted to a stroke model, where NPs penetration into the brain was studied and analysed after its systemic administration.

All types of NPs assayed were able to cross the BBB and were endocytosed by neurons; however, the SH-NPs obtained by M2 are lightly more efficient in the rate of penetration than those obtained by M1. There were not visible differences between coated and non-coated NPs obtained by both gelation methods. This may be due to the fact that not only the size, shape and charge of NPs, but also its chemical structure influences its cellular capture by endocytic mechanisms.

1. Introduction

Many biological drugs with proven neuroprotective capacity are unable to cross the blood brain barrier (BBB), making its use unfeasible in neuro-regenerative therapies. Interestingly, the administration of peptides and proteins is often a highly effective treatment of these diseases or their symptoms at the same time that biologic medicines increasingly gain more space in our society [1]; unfortunately, there are some limitations to its therapeutic use because they require intravenous administration, which leads to low biodistribution and quick clearance [2]. In this sense, the development of nanocarrier systems that work as Troy horses transporting these drugs from circulation to neurons is a promising tool to allow the systemic utilization of them in most types of brain diseases [3].

Stroke is a leading cause of death and long-term disability worldwide [4,5]. Whereas two-thirds of stroke deaths occur in less developed countries [6], this disease is the second most common cause of death in Europe [7]. There are two major types of stroke, haemorrhagic stroke and ischemic stroke; the last one being the most frequent (80–85%). This type of stroke is caused by a blood clot or by the narrowing of a blood vessel blocking oxygen and nutrients supply to the infarcted area. Nowadays, the most common treatment consists of the administration of the tissue plasminogen activator (tPA) that works in the acute phase of the stroke dissolving the clot and improving blood flow. However, if it is not administered within the first hours after the stroke, it does not prevent either the recanalization of the vessels or the further neurodegeneration due to the damage occurring during the reperfusion period [8]. In fact, 10–40% of the patients treated with tPA develop a haemorrhagic transformation, increasing mortality and morbidity [9,10]. Accordingly, stroke treatments should act not only on

* Corresponding author at: Department of Experimental Biology, Building B3, Office 340, Campus de Las Lagunillas, S/N-23071 Jaén, Spain.
E-mail address: apeinado@ujaen.es (M.Á. Peinado).

https://doi.org/10.1016/j.eurpolymj.2019.01.030
Received 31 October 2018; Received in revised form 11 January 2019; Accepted 13 January 2019
Available online 16 January 2019
0014-3057/

restoration of normal circulation but also on neuronal protection in the reperfusion period, reducing or ameliorating the events that trigger neuronal damage.

In the past 20 years, a large number of clinical trials searching for neuro-protectants against the brain damage produced by stroke and neurodegenerative disorders has been developed with disappointing outcomes [11]. These difficulties are mainly due to the scarce permeability of the BBB; interestingly, near 100% of the large neurotherapheutic molecules and 98% of the small drugs never reach its target in the cerebral parenchyma. Consequently, the BBB acts as a bottleneck in relation to the development of brain drugs [12]. As previously mentioned, one of the strategies proposed to solve this difficulty is the use of nanoscale drug delivery systems, which includes liposomes, micelles or nanoparticles (NPs), often modified with different ligands on their surface to increase the selectivity of the delivery [13].

Nanoparticles (NPs) are exogenous synthetic structures with nanoscale dimensions, which have raised enormous interest toward biological applications. Owing to their comparatively large size, the cellular uptake of NPs is necessarily different from other types of molecules. For example, while most molecules are unable to be internalized by cells efficiently on their own (*vide supra*), NPs are actively incorporated into the cell, via different endocytic pathways [14]. NPs have been found to have larger activated surface area than other physical forms to support drug-loading capacity, and they also have a long useful life and good permeability through epithelia; moreover, its shape and size as well as its easy transportation inside the body make them very useful to this end [15]. Moreover, NPs could improve the biological activity of many neurotherapeutic drugs, due to the increase of its surface area, which leads to better bioavailability [16].

Sodium hyaluronate (SH) is a versatile natural anionic polysaccharide, with a wide spectrum of physicochemical and functional properties, which makes it very suitable for the synthesis of NPs. This polymer is located in the extracellular matrix and connective tissue of vertebrates, being highly biocompatible [17] and quite suitable for pharmacological use. SH has several functions within the organism, including its role in tissue structure, energy storage or cell recognition [18]. Consequently, the nanostructures obtained with SH should be able to avoid the immune system and cross some of the barriers that the body uses to prevent the penetration of foreign or unwanted substances, such as the previously mentioned BBB. Among the methods used to prepare SH-NPs, the ionic gelation technique is widely preferred [19–21]. The formation of particles using ionic gelation is not aggressive and avoids demanding organic solvents and high temperatures, allowing effective encompassing of delicate molecules without any damage and loss [22]. This method depends principally on ionic interactions between anionic chains of SH and cationically-charged polyions, e.g. calcium as a cross linker [23]. Besides encapsulation and drug loading, SH-NPs can also be coated with certain materials like chitosan or lipids, thus enhancing their specificity as carriers providing better targeting [24]. Polyionic nano-complexes composed of polyanions and opposite polycations have been found to have a great potential in biomedical and nano-biotechnological applications, including controlled drugs release and gene transfection [23,25,26].

The objective of this study is to design and develop hyaluronate-based NPs able to transport large therapeutic molecules to cerebral parenchyma affected by neurodegenerative diseases such as ischemic stroke. NPs will be prepared using two different ionic gelation methods; in addition, they will be coated layer-by-layer with chitosan and glycerol tripalmitin to obtain particles of adequate size, chemical structure and charge to achieve the intended purpose. In addition, the ability of these NPs to cross the BBB and to deliver the transportation drugs into the neurons of control animals and after an experimental model of stroke has been assessed.

2. Experimental

2.1. Materials

Grape seed oil and Tween® 80 were obtained from Guinama (Valencia - Spain). Sodium Hyaluronate (1.0–1.5 MDa) was purchased from Fagron (Barcelona - Spain). Calcium Chloride, Chitosan (low molecular weight), Glacial Acetic acid, Glycerol tripalmitin, Rhodamine-123, 2,3,5-Triphenyltetrazolium chloride and PBS were obtained from Sigma-Aldrich Quimica SL (Madrid - Spain). Dichloromethane was purchased from VWR (Barcelona - Spain), ketamine (Imalgene 100 mg/ml) from (Merial Laboratorios S.A., and xylacine (Rompun®) from Bayer. Uranyl Acetate was obtained from Electron Microscopy Sciences (Hatfield, PA - USA), and distilled water was prepared by a Millipore (Billerica, MA, USA) system.

2.2. Methods

2.2.1. Synthesis of NPs

In order to compare and obtain the best NPs synthesis method that meets our objectives, two NPs ionic gelation methods have been developed: external (M1) and emulsification/external gelation (M2) techniques. The base of the NPs obtained by M1 and M2 methods is sodium hyaluronate (SH) as a common polymer. In addition, they also share common coatings, but on the contrary, they present differences in the elaboration of their core.

According to external gelation technique (M1), the NPs of SH (M1 SH-NPs) are prepared following a modified ionic gelation method [27,28] during which they are dispersed in 100 mL of water with rhodamine: 0.02% (w/v) SH and 0.5% (w/v) Tween® 80, under mechanical shaking at 1200 rpm for 5–10 min until a homogeneous dispersion is achieved. Subsequently, the stirring speed is increased to 1600 rpm, 0.25% (w/v) calcium chloride is added, and the stirring continues at 1200 rpm for 2 h.

Emulsification/external gelation method (M2) to make NPs of SH (M2 SH-NPs) is based on the formation of a water-oil emulsion (W/O). To get this type of NPs, grape seed oil is dispersed in 40 mL of water with rhodamine, 0.06% (m/v) SH, and 0.6% (w/v) Tween® 80 at a temperature of 40 °C. 100 mL of grape seed oil is heated to 40 °C; then the aqueous phase is added to the oil at a speed of 1200 rpm for 10 min. Subsequently, 5 mL of a 5% calcium chloride solution (w/v) is incorporated at a speed of 1600 rpm for about 10 min, continuing the stirring at 1200 rpm for 2 h.

Both types of SH-NPs were also subjected to coating with chitosan (CH) and glycerol tripalmitin (GT). For coating, 1% chitosan solution is used, in which 1 mL of glacial acetic acid 1% (v/v) is previously added. The solution was acidified to facilitate the dissolution of chitosan before coating. This solution is mixed in equal parts with the dispersion of the SH-NPs, keeping the mixture in magnetic stirring for 2 h. Then, CH-coated SH-NPs are subjected to a lipid coating with GT, a biocompatible triglyceride present in the human body as fat [29], which lipidic character facilitates the penetration of the NPs through the BBB. GT (0.1% (m/v) is dissolved in dichloromethane and added to 10 mL of the colloidal dispersion of SH-NPs, maintained under magnetic stirring until complete evaporation of the solvent.

2.2.2. Particle size, polydispersity and Zeta potential measurement

The size distribution and the size of the NPs were determined by mean of dynamic light scattering with Non-invasive Backscattering Optics (NIBS), measured after dispersing them in water. For this, the mean particle size was determined by Malvern Zetasizer Nano ZS®; Malvern Instruments Ltd, Malvern, UK), at 25.0 °C ± 0.5 °C. The average size is expressed in nanometers (nm).

The measurement of the charge has been carried out in the same device (Malvern Zetasizer Nano ZS®; Malvern Instruments Ltd, Malvern, UK) using electrophoretic light scattering and a molecular weight

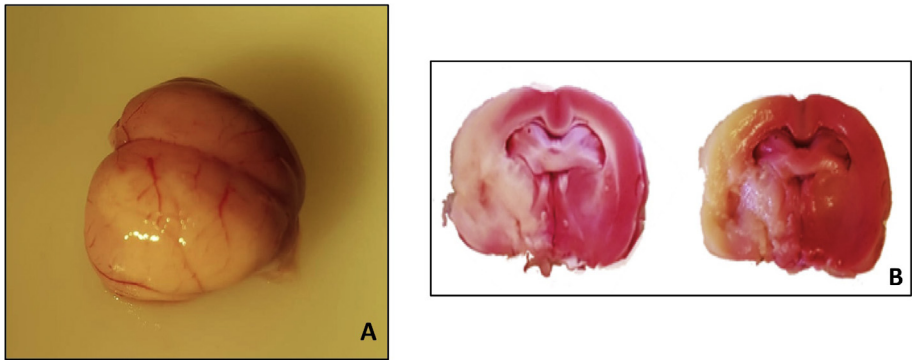

Fig. 1. A: Brain submitted to MCAO showing the infarct area in the left hemisphere as a most inflamed and pale area. B: Brain sections stained with TTC showing the infarcted area; as can be seem, it appears white in contrast to the red-stained no affected areas. (For interpretation of the references to color in this figure legend, the reader is referred to the web version of this article.)

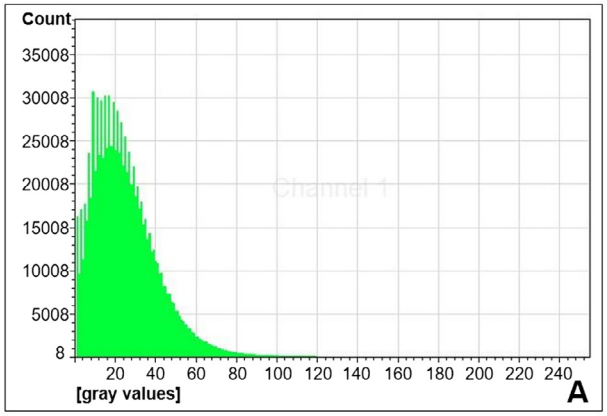

Channel 1	
	ROI1
Area	52686.58 (µm)²
Mean Value	24.83 gray values
Pixel Count	1029204
Pixel Sum	25551611
Maximum	255.00 gray values
Minimum	0.00 gray values
Variance	395.05 gray values
Standard Deviation	19.88 gray values
Average Deviation	13.79 gray values
Maximum Peak	230.17 gray values
Maximum Valley	24.83 gray values

B

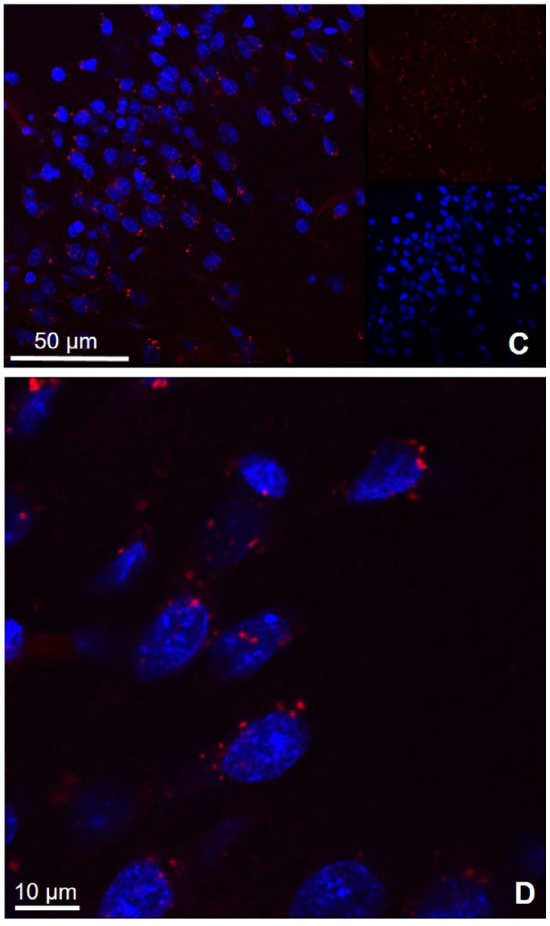

Fig. 2. Rhodamine-fluorescent-NPs gray values of a predetermined area of the visual field obtained using the Leica advanced software AF. This software allows to estimate the distribution (A) and quantification (B) of the rhodamine fluorescent levels (grey values) associated to the different NPs assayed. Mean value parameter inform about the rhodamine fluorescence levels of the brain parenchyma quantified in an area of the confocal image captured at a pre-determined magnification (C and D). The gray values were always obtained in equivalent brain areas (parietal cortex) and using the same magnification.

analyzer with static light scattering. The colloidal dispersion is introduced partially diluted. Zeta potential is expressed in millivolts (mV).

In both cases, Malvern Instruments software was used; this software adapts automatically to the attenuation of the dispensing. Three measurements of each sample were made. These three measurements are the average among 10 to 15 repetitions depending on the sample.

2.2.3. Microphotographic analysis

NPs are arranged in the suitable supports (grids) for viewing. The devices used for this study have been Transmission Electron Microscope (TEM): CARL. ZEISS LEO 906E and Scanning Electron Microscope (SEM): GEMINI (FESEM) CARL ZEISS. The Scientific Instrumentation Center (CIC) of the University of Granada (Spain) has facilitated both microscopes.

For TEM, the sample was prepared via negative staining. The dispersion was incubated in a grid with carbon support film for 5 min in a Petri dish and contrasted with 1% uranyl acetate in aqueous solution. The magnification of the images are showed by mean of a scale bar of 5 µm, 1 µm, 500 nm and 100 nm respectively.

For SEM, a drop of the colloidal dispersion of NPs was deposited on a corresponding support for the FESEM (pin stub mount) allowing it to dry at room temperature. Subsequently, they were sputtered with carbon with Carbon Coater (Polaron CC7650). The magnification of the

Table 1
Size, polyspersion and ζ-potential of the different types of NPs.

Sample	Size Average (nm)	Polydispersion	ζ-Potencial (mV)
M1 SH-NPs	65.69 ± 0.98	0.89 ± 0.15	−24.03 ± 6.70
M2 SH-NPs	55.92 ± 7.60	0.84 ± 0.22	−26.70 ± 9.20
CH-M1 SH-NPs	193.66 ± 10.37	0.34 ± 0.07	47.50 ± 1.61
CH-M2 SH-NPs	163.73 ± 14.05	0.53 ± 0.11	29.67 ± 1.41
GT-CH-M1 SH-NPs	248.06 ± 6.17	0.46 ± 0.09	27.93 ± 1.50
GT-CH-M2 SH-NPs	243.16 ± 6.02	0.37 ± 0.03	17.88 ± 2.02

images are showed by means of a scale bar of 500 nm.

2.2.4. Experimental animals

The experimental procedures to assess the *in vivo* brain penetration of the different NPs elaborated have been carried out in adult male Wistar rats (Charles River). All procedures have been carried out in the Centre for Animal Production and Experimentation of the University of Jaen (CPEA) and previously approved by the local Animal Care Committee and performed in compliance with the Spanish legislation and in accordance with the EU Directive 2010/63/EU (2010).

Animals were distributed into two experimental groups: animals subjected to a stroke model by occlusion of the middle cerebral artery (MCAO group), and animals that underwent the same surgical procedures without filament occlusion of the artery (control group). This experimental design was made in order to identify possible differences in the ability of NPs to reach the cerebral parenchyma, in both control and stroke animals, given that the last group could present a disrupted BBB [30].

2.2.5. Stroke model

The experimental procedure consisted on a slight modification of the model of the occlusion of the middle cerebral artery (MCAO) [31]. In brief, anaesthesia was induced by i.p. injection of 100 mg/kg ketamine and 10 mg/kg xylazine in mixture. Rectal temperature was maintained at 37.51 °C by using a feedback-controlled heating pad. Under a stereo zoom microscope, the right common, external, and internal carotid arteries were dissected from connective tissue through an incision in the neck midline. A 23-mm segment of 3–0 nylon monofilament suture 3–4 mm coating for rats commercially available (Doccol Corp., Redlands, CA, USA) was inserted into the stump of the right common carotid artery and advanced into the internal carotid artery ~18–20 mm from the bifurcation to occlude the origin of the middle cerebral artery. The suture was removed after 45 min of occlusion. A Laser-Doppler flow probe (tip diameter 1 mm) attached to a flowmeter (PeriFlux 5000; Perimed AB, Stockholm, Sweden) was located over the thinned skull in the MCAO territory (4 mm lateral to bregma) to obtain a continuous measure of relative cerebral brain flow during the experiment. Only animals with a cerebral blood flow reduction over 60% were included in the study. After surgery and recovery, the rats were returned to their home cages and sacrificed 2 h after reperfusion. As previously mentioned, control-operated rats underwent the same experimental procedures, but without filament occlusion.

2.2.6. Histology and microscopy

Histology and confocal microscopic analysis were carried out in the Research Support Services of the University of Jaén (SCAI).

To assess the efficiency of uptake of NPs into the brain parenchyma, rhodamine-123-fluorescence-labelled-NPs prepared following methods 1 and 2, not coated (M1 SH-NPs and M2 SH-NPs) or coated (GT CH M1 SH-NPs and GT CH M2 SH-NPs) were injected throughout the radial vein of the tail at the onset of reperfusion, in both control and stroke animals. After sacrifice, the brains of all injected animals were removed and cut into 2 mm-thick sections; in addition, some sections from the

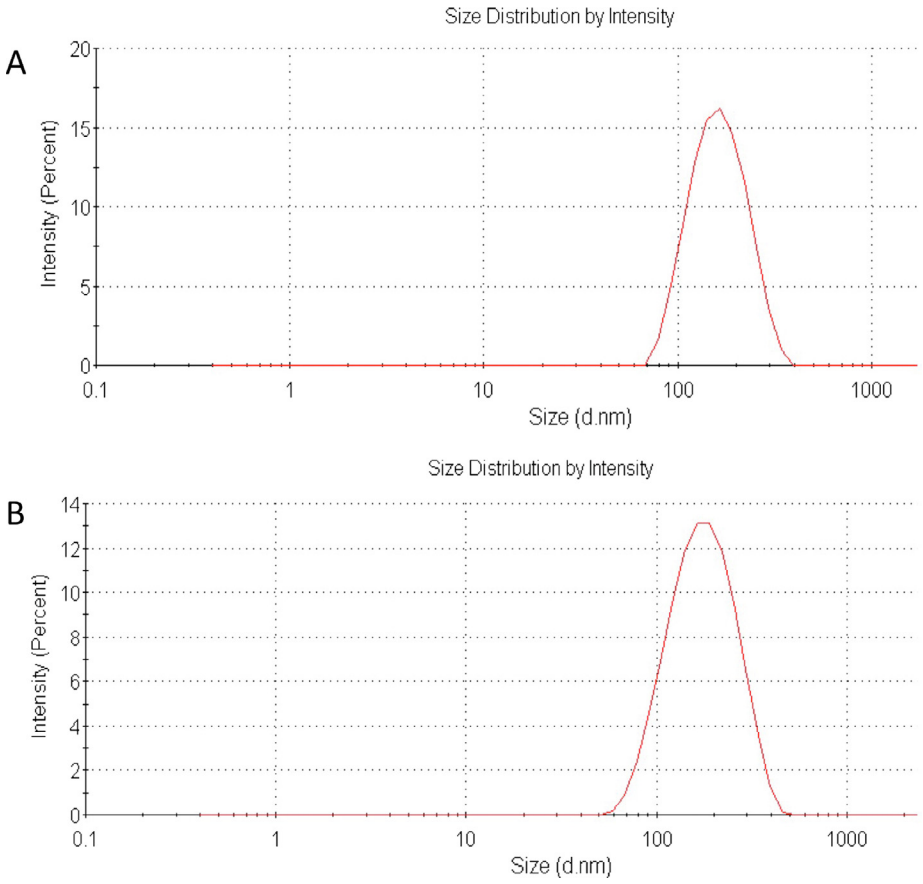

Fig. 3. Size distribution of the NPs: A: Size distribution Method 1 with covers (GT CH M1 SH-NPs). B: Size distribution Method 2 with covers (GT CH M2 SH-NPs).

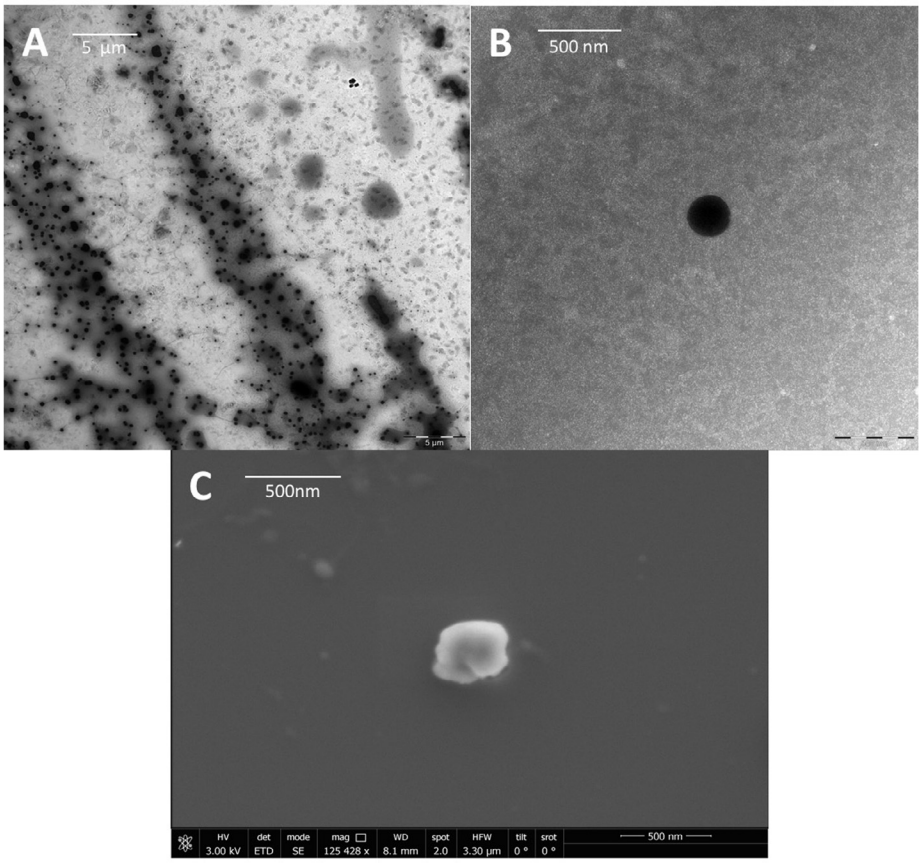

Fig. 4. Microscopy characterization of coated sodium hyaluronate nanoparticles by method 1 (GT CH M1 SH-NPs). A. TEM. Scale 5 µm. B. TEM. Scale 500 nm. C. SEM. Scale 500 nm.

brains of the MCAO group were stained with triphenyltetrazolium chloride monohydrate (TTC) [32] to visualize the infarcted area, which appears white in contrast to the red-stained normal areas (Fig. 1).

Other sections from the brains of both control and MCAO groups were frozen and cut into 20 µm slices with a cryostat (Leica CM1950). Afterward, slices were washed twice in potassium phosphate buffer (pH 7.4) for 15 min and stained with DAPI (Sigma-Aldrich) to visualize the cell nuclei. Finally, the slices were mounted on slides for examination under confocal laser scanning microscope (Leica TCS SP5 II). Cell nuclei were visualized in blue due to DAPI staining (Excitation 358, Emission 529), whereas NPs appeared in red due to rhodamine (Excitation 507, Emission 525); so the biodistribution of the different types of NPs within the brain parenchyma in both experimental groups could be determined.

Finally, an estimation of the rhodamine fluorescence of each type of NPs was automatically performed in the different brain samples using the Leica advanced software AF. This software enables to analyse the distribution and quantification of the fluorescent levels (estimated as grey values) of the different NPs assayed in a previously determined brain tissue area of the microscopy visual field. For all histological sections, identical magnification and equivalent areas of the parietal cortex was always used. An example of the distribution and quantification of the rhodamine-fluorescence associated to the NPs obtained with this software is shown in Fig. 2.

3. Results and discussion

3.1. Physicochemical characterization

The macroscopic analysis of the dispersion of the NPs shows that there is no presence of aggregates or sediments. Both methods have a slight whitish color that is accentuated in the case of method 2. Although a slight turbidity is characteristic, the colloidal dispersions are homogeneous and stable in all cases and throughout the study. According to the information provided by Decuzzi [33], NPs with a size between 100 and 200 nm are easily captured by endocytosis, and particles greater than 300 nm are captured by phagocytosis. Therefore, the ideal size of these nanocarriers should be below 300 nm. Table 1 shows the particle size, polyspersion, and Zeta potential of the different types of NPs studied. The results show that the size of the SH-NPs in each case is below 100 nm, in particular, 65.69 ± 0.98 nm for M1 SH-NPs and 55.92 ± 7.60 nm for M2 SH-NPs. However, as expected, this size is increased by around 300% by coating the NPs with chitosan. This increase in size, besides the own contribution of the chitosan layer, is also influenced by the electric charge of the particles, which become positive (with a value of more than 30mv) after the coating (above −25mv before coating). The addition of the glycerol-tripalmitin layer to the coated NPs (GT-CH SH-NPs) offers a definitive size of 248.06 ± 6.17 and 243.16 ± 6.01 for M1 and M2 methods respectively. These sizes, based on the above layer-by-layer procedure, are suitable for the purpose for which they have been designed. On the other hand, polydispersity is inherent in the proposed synthesis methods, as corroborated by the data recorded in Table 1, in which the polydispersion decreases with the coating. In fact, the values of polydispersion in the initial nanoparticle synthesis (before coating) are high for both M1 and M2; one of the reasons for these data may be its small size. These small NPs can easily form agglomerates, although they do not have much relevance because the polyspersion subsequently decreases with the coating. Definitive particle size analysis (Table 1) showed a unimodal size distribution (Fig. 3) in both cases, with a mean diameter of 248.06 ± 6.17 nm for GT-CH M1 SH-NPs and 243.16 ± 6.02 nm for GT-CH M2 SH-NPs. Hence, both ionic gelation methods for the

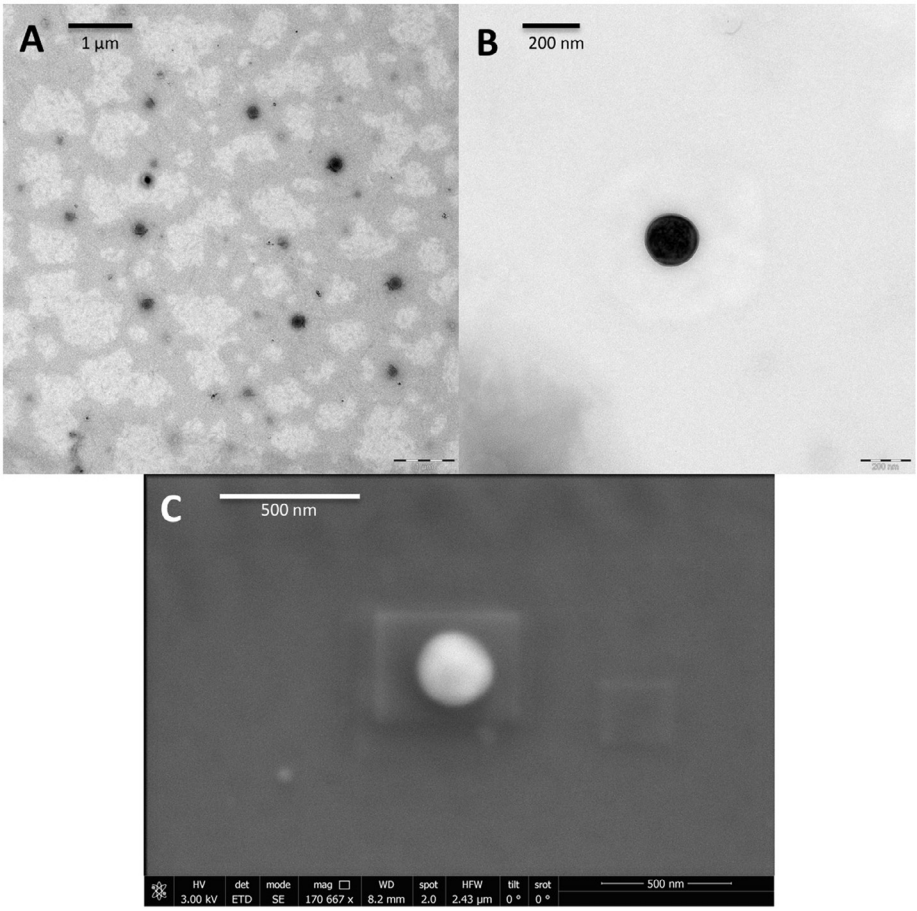

Fig. 5. Microscopy characterization of coated sodium hyaluronate nanoparticles by method 2 (GT CH M2 SH-NPs). A. TEM. Scale 1 µm. B. TEM. Scale 200 nm. C. SEM. Scale 500 nm.

preparation of SH-NPs and the layer-by-layer coating with chitosan and glycerol tripalmitin were found to be effective techniques.

Zeta potentials were recorded for the different types of NPs directly after synthesis and modified surface charge (Table 1). The main objective is that NPs keep to Fick's Law [34], essential to allow them to pass through cell membranes through passive diffusion [35]. Ideal conditions entail that the NPs have a certain size and a slight positive charge to facilitate their penetration. Initially, it is observed that SH-NPs present a negative charge of -24.03 ± 6.70 mV for method 1 and -26.70 ± 9.20 mV for method 2. After being coated with chitosan, which is a cationic polysaccharide, the particles undergo a change in the sign of the charge, which increases in absolute value to 47.50 ± 1.61 mV and 29.67 ± 1.41 mV for CH M1 SH-NPs and CH M2 SH-NPS, respectively. We also detected that the greatest changes in size and charge of NPs occur with this coating. In the third and last coating, the lipids present a negative charge, enough to allow them to adhere to the surface of the NPs (now positive), but not to reverse their charge as in the previous case. Thus, the NPs remain positive, although the Zeta potential decreases in absolute value because layer-by-layer assembly technique relies on electrostatic deposition of oppositely charged polyelectrolytes on the nanocarrier surface. In short, we obtain 27.93 ± 1.50 mV GT-CH M1 SH-NPs and 17.88 ± 2.02 mV GT-CH M2 SH-NPs. On the one hand, these absolute values help to guarantee the technological stability of the colloidal systems during their conservation. On the other hand, chitosan (cationic polysaccharide) coating-based SH-NPs led to the conversion of the NPs' surface charge for enhanced cell internalization. Additionally, a lipid coating was made in order to improve the permeation of nanocarriers through the BBB since favors its liposolubility without greatly altering its charge. In fact, proteoglycans, mucopolysaccharides, glycolipids and flucoproteins with sulfates and sialic acids confer to cell plasma membrane a negative charge at physiological pH; thus, electrostatic interaction between the positively charged part of the NPs and the negatively charged of the cell membrane could favors its adsorption and transport throughout endothelial cells [36].

3.2. Morphology study

Fig. 4 shows GT-CH M1 SH-NPs microphotographs obtained by TEM (Fig. 4A and B) and SEM (Fig. 4C). In the first image (Fig. 4A), particles of different sizes can be observed. No significant differences in morphology and polydispersity on the size distribution were found among them. Worth mentioning, it is a polyspersed colloidal system, as shown by the results in the previous section. The following image (Fig. 4B) focuses on a NP with high resolution that exhibits edges and a slightly lighter surface, most likely corresponding to the different coating materials. The size falls within the range of average results discussed above and shows spherical shape with a defined limit. According to Huiyi and collaborators [37], the spherical shape could serve for the maintenance of the textural quality [20].

In Fig. 4C, using SEM microscopy, the NP is not as uniform in its shape, and the sphericity has evidently been slightly lost, most likely due to the coatings. Its surface is not smooth but rough and spongy, although there are no evident pores on the surface, which is a positive sign because high porosity is associated with a fast and easy diffusion of water and other fluids in and out of the matrix, and subsequently with cell leakage [38,39].

In Fig. 5, spherical and slightly polyspersed NPs can be seen as black

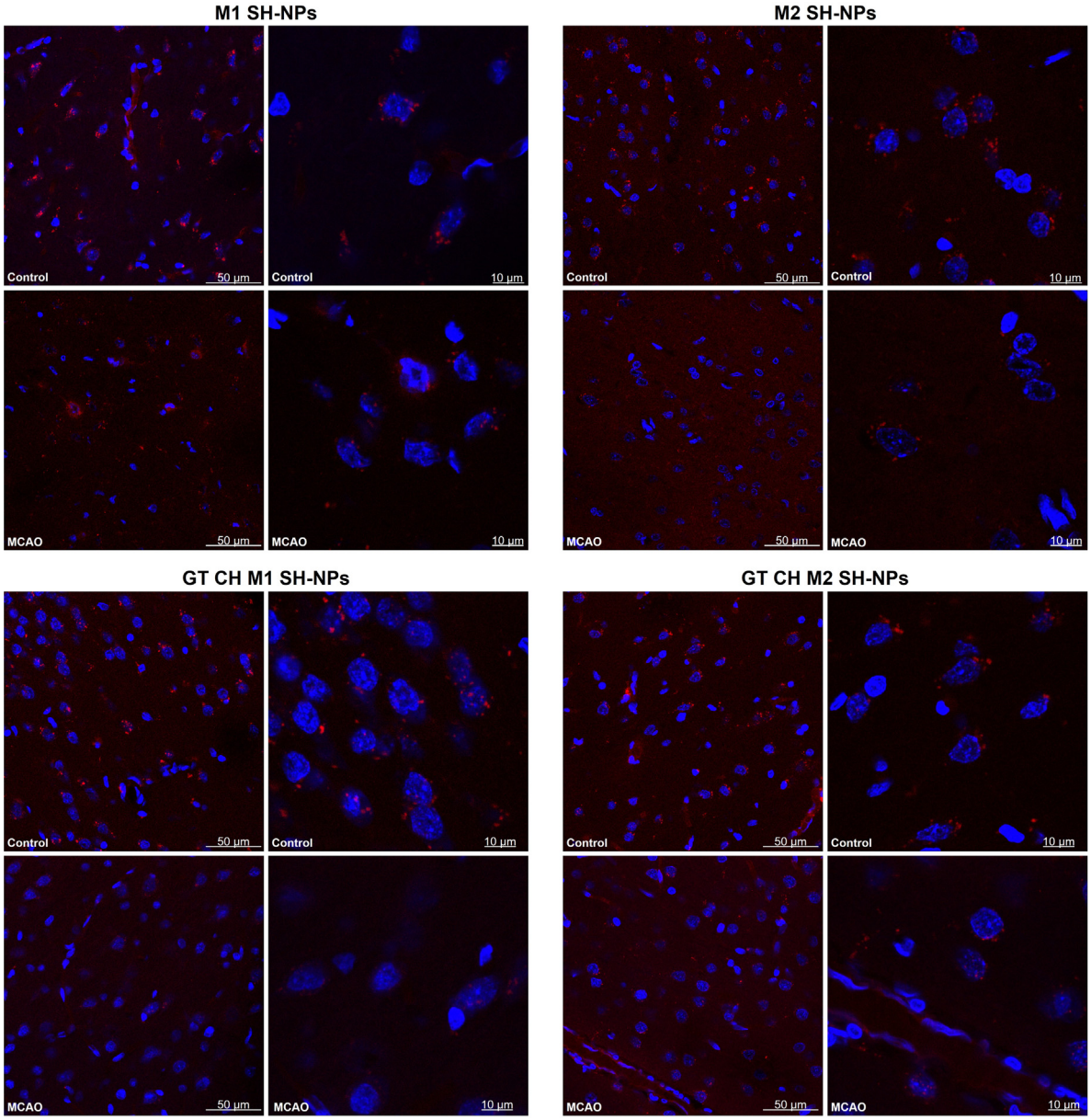

Fig. 6. Histological sections of the brains, from control and MCAO animals at the parietal cortex area, showing the different rhodamine-fluorescent-NPs assayed located in the vascular wall but mainly in neuron cytoplasm.

spots for GT-CH M2 SH-NPs. By focusing on an isolated NP (Fig. 5B), a darker core and clear edges are clearly distinct, perhaps due to the coating used. Its size is around 200 nm.

Finally, in the third image (Fig. 5C), a completely spherical NP is observed. It seems that the coating around the surface of the SH core is different to the previous methods, in which NPs do not show a perfect uniformity in their sphericity. In this case, there is no presence of porosity on the NP's smooth surface. The coating in this method is more uniform than in the previous method.

3.3. Estimation of the rhodamine fluorescence of NPs in the cerebral parenchyma.

Animals from both control and MCAO groups were injected with the different SP-NPs treatments. Fig. 6 shows an estimation of the gray levels (rhodamine fluorescence levels) for the four types of SP-NPs assayed (M1 SH-NPs, GT-CH M1 SH-NPs, M2 SH-NPs and GT-CH M2 SH-NPs) in the cerebral parenchyma of the two rat groups. The NPs, which were administrated to the animals through the tail vein 2 h before sacrifice, appear under the confocal microscopy as red vesicles due to rhodamine fluorescence. Every type of NPs crossed the BBB being captured later by neurons. As shown, neurons exhibit NPs mainly allocated in their cytoplasm as vesicles placed around the nuclei, probably associated with the endomembrane cellular system. Less fluorescent NPs can be seen beside the endothelial cells at the lumen of the vessels and inside the vascular wall. Different receptors in endothelial cells must be involved in transcytosis mechanisms in order to allow NPs to cross the BBB [14,40] and be captured by neurons. These mechanisms should manage the trafficking of NPs inside the brain parenchyma and address its preferential accumulation in neuronal cells. Thus, different SH-receptors, like CD44, Layilin, LYVE-1, HARE/Stab2 or RHAMM in the cell surface have been described [41], which probably influence NPs penetration into cells. However, the clarifications of such mechanisms will require more investigation not only *in vivo* but also *in vitro* [3,40].

The estimation of rhodamine-fluorescence levels were evaluated in

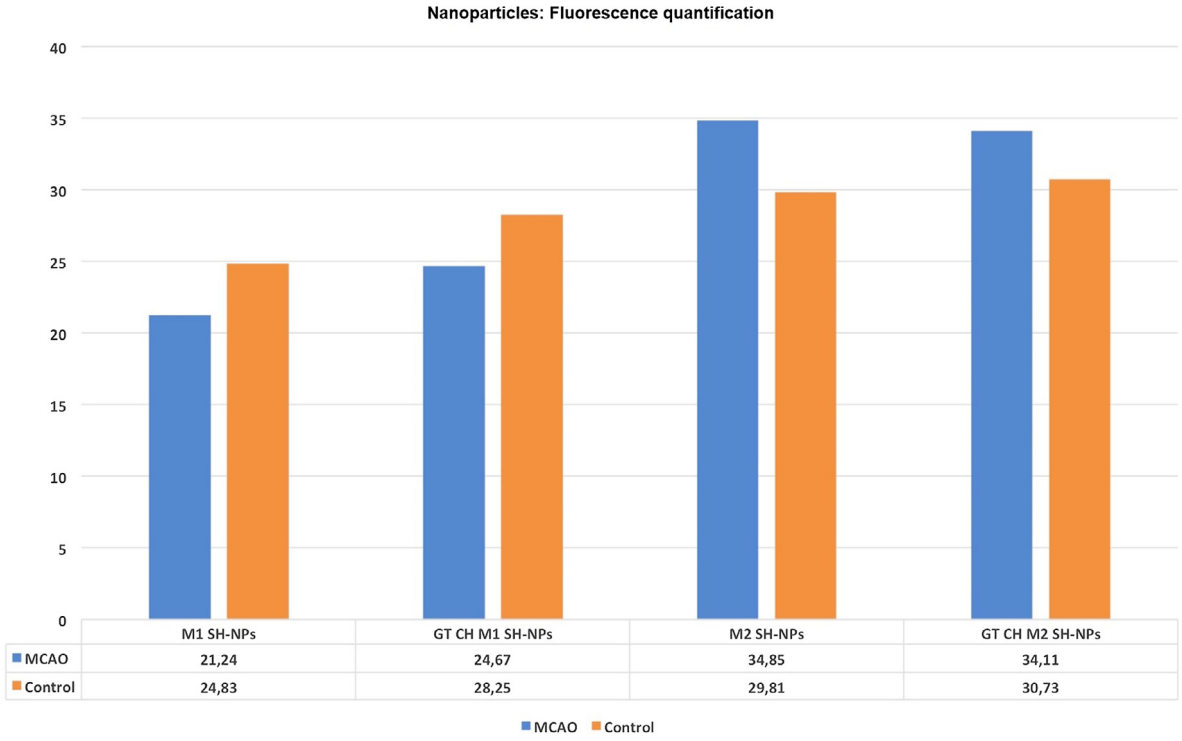

Fig. 7. Estimation of the gray mean values of the different rhodamine-fluorescence-NPs assayed in the cerebral parenchyma of both control and MCAO groups in a determined area of the parietal cortex. As can be seem M2 methods showed higher values than M1. In addition, there are hardly changes based on the NPs coat or due to the stroke.

histological sections of both control and MCAO animals using the Leica advanced software AF as was previously described. Data are shown in Fig. 7 for all NPs assayed (M1 SH-NPs, GT-CH M1 SH-NPs, M2 SH-NPs and GT-CH M2 SH-NPs). In both animal groups, M2 NPs showed better penetration in cerebral parenchyma than M1 NPs; this result must be consequence of the different composition of M1 and M2 NPs core, which influences the effectiveness of the endocytic mechanisms, even though both M1 and M2 non-coated SH-NPs present negative charge and a similar size of about 60 nm. On the other hand, we did not found remarkable differences between coated and no coated NPs. This may be because positively charged coated nanocarriers enhance membrane association, internalization and endosomal escape, whereas those not coated, despite its negative Zeta potential, have more specific and efficient uptake, particularly because they are more easily targeted with specific cell ligands [3,14,24].

Finally, the absence of differences between control and MCAO groups in both M1 and M2 methods is notable, possibly because 2 h after a stroke, the BBB is still intact, and has not had enough time to undergo changes in permeability [30].

4. Conclusion

Ionic gelation methods were found to be effective techniques for the preparation of SH-NPs. In addition, the layer-by-layer coating of the SH nanoparticles with chitosan and glycerol tripalmitin has given rise to particles of adequate size of about 245 nm and surface charge of about 32 mV to be used as delivery system to transport large neurotherapheutic molecules to cerebral parenchyma.

As this study demonstrates, all types of NPs assayed are able to cross the BBB and are endocytosed by neurons; although the SH-NPs obtained by M2 are lightly more efficient than those obtained by M1, there were no visible differences between coated and not coated NPs for each method. This may be because not only the size, shape and charge of NPs, but also its chemical structure influences its cellular capture by endocytic mechanisms. Finally, any type of NPs show differences in the penetration level between controls and MCAO animals, probably due to the fact that 2 h after stroke the BBB is still intact.

Acknowledgement

We gratefully acknowledge financial support from project BFU2016-80316-R of Ministerio de Economía y Competitividad (MEC).

Conflicts of interest

There are no conflicts of interest.

References

[1] S. Peralta, M.E. Morales, M.A. Ruiz, Estudio bibliometrico sobre el impacto de los medicamentos biosimilares, Ars Pharm. 58 (2017) 103–106.
[2] F.M. Steinberg, J. Raso, Biotech pharmaceuticals and biotherapy: an overwiew, J. Pharm. Sci. 1 (1998) 48–53.
[3] A. Vilella, B. Ruozi, D. Belletti, F. Pederzoli, M. Galliani, V. Semeghini, F. Forni, M. Zoli, M.A. Vandelli, G. Tosi, Endocytosis of nanomedicines: the case of glycopeptide engineered PLGA nanoparticles, Pharmaceutics 7 (2015) 74–89.
[4] B. Cai, Y. Lin, X.H. Xue, L. Fang, N. Wang, Z.Y. Wu, TAT-mediated delivery of neuroglobin protects against focal cerebral ischemia in mice, Exp. Neurol. 227 (1) (2011) 224–231.
[5] X. Song, R. Xu, F. Xie, H. Zhu, J. Zhu, X. Wang, Hemin offers neuroprotection through inducing exogenous neuroglobin in focal cerebral hypoxic-ischemia in rats, Int. J. Clin. Exp. Pathol. 7 (5) (2014) 2163–2171.
[6] C. Warlow, C. Sudlow, M. Dennis, J. Wardlaw, P. Sandercock, Stroke, Lancet 362 (9391) (2003) 1211–1224.
[7] M. Nichols, N. Townsend, R. Luengo-Fernandez, J. Leal, A. Gray, P. Scarborough, M. Rayner, European Society of Cardiology, Sophia Antipolis P10, 2012.
[8] R.S. Pandya, L. Mao, H. Zhou, S. Zhou, J. Zeng, A.J. Popp, X. Wang, Central nervous system agents for ischemic stroke: neuroprotection mechanisms, Cent. Nerv. Syst. Agents Med. Chem. 11 (2) (2011) 81–97.
[9] L.A. Beslow, S.E. Smith, A. Vossough, D.J. Licht, S.E. Kasner, C.G. Favilla, A.R. Halperin, D.M. Gordon, C.I. Jones, A.J. Cucchiara, R.N. Ichord, Hemorrhagic transformation of childhood arterial ischemic stroke, Stroke 42 (4) (2011) 941–946.
[10] V. Terruso, M. D'Amelio, N. Di Benedetto, I. Lupo, V. Saia, G. Famoso, M.A. Mazzola, P. Aridon, C. Sarno, P. Ragonese, G. Savettieri, Frequency and determinants for hemorrhagic transformation of cerebral infarction, Neuroepidemiology 33 (3) (2009) 261–265.

[11] Z. Yu, N. Liu, J. Liu, K. Yang, X. Wang, Neuroglobin, a novel target for endogenous neuroprotection against stroke and neurodegenerative disorders, Int. J. Mol. Sci. 13 (6) (2012) 6995–7014.
[12] W.M. Pardridge, The blood–brain barrier: bottleneck in brain drug development, NeuroRx 2 (2005) 3–14.
[13] Y. Chen, L. Liu, Modern methods for delivery of drugs across the blood–brain barrier, Adv. Drug Deliv. Rev. 64 (2012) 640–665.
[14] J. Mosquera, I. García, L.M. Liz-Marzán, Cellular Uptake of Nanoparticles versus Small Molecules: A Matter of Size Accounts of Chemical Research 51 (2018) 2305–2313.
[15] A. Almalik, H. Benabdelkamel, A. Masood, I.O. Alanazi, I. Alradwan, M.A. Majrashi, A.A. Alfadda, W.M. Alghamdi, H. Alrabiah, N. Tirelli, A.H. Alhasan, Hyaluronic acid coated chitosan nanoparticles reduced the immunogenicity of the formed protein corona, Sci. Rep. 7 (2017) 10542.
[16] B.S. Zolni, A. González-Fernández, N. Sadrieh, M.A. Do-brovolskaia, Nanoparticles and the immune system, Endocrinology 151 (2010) 458–465.
[17] S. Al-Qadi, A. Grenha, C. Remuñán-López, Microspheres loaded with polysaccharide nanoparticles for pulmonary delivery: preparation, structure and surface analysis, Carbohydr. Polym. 86 (2011) 25–34.
[18] M.L. Hans, A.M. Lowman, Biodegradable nanoparticles for drug delivery and targeting, Curr. Opin. Solid State Mater. Sci. 6 (2002) 319–327.
[19] M.J. Martin, F. Lara-Villoslada, M.A. Ruiz, M.E. Morales, Effect of unmodified starch on viability of alginate-encapsulated Lactobacillus fermentum CECT5716, Food Sci. Technol. 53 (2013) 480–486.
[20] M. Sanchez, M. Ruiz, A. Lasserrot, M. Hormigo, M.E. Morales, An improved ionic gelation method to encapsulate Lactobacillus spp. bacteria: protection, survival and stability study, Food Hydrocoll. 69 (2017) 67–75.
[21] A.L. Pinho-Neves, C. Cardoso, L. Müllera, H. Gracher, N. Cabral, H. Karine, Factorial design as tool in chitosan nanoparticles development byionic gelation technique, Colloids Surf. A Physicochem. Eng. Asp. 445 (2014) 34–39.
[22] W. Fan, W. Yan, Z. Xu, H. Ni, Formation mechanism of monodisperse, low molecular weight chitosan nanoparticles by ionic gelation technique, Colloids Surf. B 90 (2012) 21–27.
[23] M. Deng, B. Hu, L. Xu, Y. Liu, F. Wang, H. Zhao, X. Wei, J. Wang, K. Yi, OsCYCP1;1, a PHO80 homologous protein, negatively regulates phosphate starvation signaling in the roots of rice (Oryza sativa L.), Plant. Mol. Biol. 86 (2014) 655–669.
[24] A. Almalik, S. Karimi, S. Ouasti, R. Donno, C. Wandrey, P.J.D.N. Tirelli, Hyaluronic acid (HA) presentation as a tool to modulate and control the receptor-mediated uptake of HA-coated nanoparticles, Biomaterials 34 (2013) 5369–5380.
[25] M.F. Azevedo, F.R. Faucz, E. Bimpaki, A. Horvath, I. Levy, R.B. de Alexandre, F. Ahmad, V. Manganiello, C.A. Stratakis, Clinical and molecular genetics of the phosphodiesterases (PDEs), Endocr. Rev. 35 (2014) 195–233.
[26] Y. Gokce, C. Burcu, N. Yildiz, A. Çalimli, Z. Aktas, Ultrasonication of chitosan nanoparticle suspension: influence on particle size, Colloids Surf. A 462 (2014) 75–81.
[27] Z. Hu, X. Xia, L. Tang, Process for Synthesizing Oil and Surfactant-Free Hyaluronic Acid Nanoparticles and Microparticles, US Patent App. 20,060/040,892, 2004.
[28] B. Lupo, C. González, A. Maestro, Microencapsulación con Alginato en Alimentos. Técnicas y Aplicaciones, RVCTA 3 (2012) 130–151.
[29] C.O. Maduko, C.C. Akoh, Y.W. Park, Enzymatic interesterification of tripalmitin with vegetable oil blends for formulation of caprine milk infant formula analogs, J. Dairy Sci. 90 (2007) 594–601.
[30] A. Kassner, Z. Merali, Assessment of blood-brain barrier disruption in stroke, Stroke 46 (2015) 3310–3315.
[31] S. Ji, G. Kronenberg, M. Balkaya, K. Färber, K. Gertz, H. Kettenmann, M. Endres, Acute neuroprotection by pioglitazone after mild brain ischemia without effect on long-term outcome, Exp. Neurol. 216 (2) (2009) 321–328.
[32] S. Ansari, H. Azari, D.J. McConnell, A. Afzal, J. Mocco, Intraluminal middle cerebral artery occlusion (MCAO) model for ischemic stroke with laser doppler flowmetry guidance in mice, J. Vis. Exp. 8 (51) (2011) 2879.
[33] P. Decuzzi, R. Pasqualini, W. Arap, M. Ferrari, Intravascular delivery of particulate systems: does geometry really matter? Pharm. Res. 26 (2009) 235–243.
[34] P. Meares, The influence of penetrant concentration on the diffusion and permeation of small molecules in polymers above tg, Eur. Polym. J. 29 (1993) 237–243.
[35] J. Ritsema, E. Herschberg, S. Borgos, C. Løvmo, R. Schmid, Y. Te-Welscher, G. Storm, C. van Nostrum, Relationship between polarities of antibiotic and polymer matrix on nanoparticle formulations based on aliphatic polyesters, Int. J. Pharm. 548 (2018) 730–739.
[36] A. Jones, E.E.V. Shusta, Blood-brain barrier transport of therapeutics via receptor-mediation, Pharm. Res. 9 (2007) 1759–1771.
[37] S. Huiyi, Y. Weiting, G. Meng, L. Xiudong, M. Xiaojun, Microencapsulated probiotics using emulsification technique coupled with internal or external gelation process, Carbohydr. Polym. 96 (2013) 181–189.
[38] A. Kumar, S. Harjinder, Recent advances in microencapsulation of probiotics for industrial applications and targeted delivery, Trends Food Sci. Technol. 18 (2007) 240–251.
[39] S. Rathore, P.M. Desai, C.V. Liew, L.W. Chan, P.W. Heng, Microencapsulation of microbial cells, J. Food Eng. 116 (2013) 369–381.
[40] R. Alyautdin, I. Khalin, M.I. Nafeeza, M.H. Haron, D. Kuznetsov, Nanoscale drug delivery systems and the blood–brain barrier, Int. J. Nanomed. 9 (2014) 795–811.
[41] P.H. Weigel, Planning, evaluating and vetting receptor signaling studies to assess hyaluronan size-dependence and specificity, Glycobiology 27 (2017) 796–799.